Metallic Character of the Al 2 O 3 (0001)−(√31 × √31) R ± 9° Surface Reconstruction †

ARTICLE *in* THE JOURNAL OF PHYSICAL CHEMISTRY B · MAY 2001

Impact Factor: 3.3 · DOI: 10.1021/jp003587c

2 AUTHORS, INCLUDING:

Emily A.A. Jarvis
Loyola Marymount University
22 PUBLICATIONS **407** CITATIONS

SEE PROFILE

Metallic Character of the Al_2O_3(0001)-($\sqrt{31} \times \sqrt{31}$)$R \pm 9°$ Surface Reconstruction†

Emily A. A. Jarvis and Emily A. Carter*

Department of Chemistry and Biochemistry, Box 951569, University of California, Los Angeles, California 90095-1569

Received: October 2, 2000; In Final Form: December 29, 2000

The basal (0001) surface plane of α-Al_2O_3 has been extensively studied both by experimental techniques and applications of theory. Although this surface is not easily created upon cleavage, it grows in during aluminum oxidation and has been shown to be one of the lowest energy surfaces of alumina. Upon heating under vacuum, this (0001) surface of α-Al_2O_3 undergoes a series of reconstructions. The final structure obtained at ∼1700 K is an air-stable termination known as the ($\sqrt{31} \times \sqrt{31}$)$R \pm 9°$ reconstruction. Alternatively, this reconstructed surface can also be obtained at lower temperatures by aluminum deposition on a clean Al_2O_3 (1 × 1) basal plane surface. Applying density functional theory within the generalized gradient approximation to a model surface, we show that the transformation from the (1 × 1) termination to ($\sqrt{31} \times \sqrt{31}$)$R \pm 9°$ is accompanied by a dramatic change in the band gap associated with the ceramic's surface. Specifically, the (1 × 1) termination is insulating for both surface and deeper "bulk-like" atoms, while the ($\sqrt{31} \times \sqrt{31}$)$R \pm 9°$ termination results in a metallic surface aluminum coating that behaves very much like an aluminum (111) surface. Although some experimental evidence for the ($\sqrt{31} \times \sqrt{31}$)$R \pm 9°$ metallic surface states exists, it has generally been ignored, and both the (1 × 1) and ($\sqrt{31} \times \sqrt{31}$)$R \pm 9°$ terminations are commonly treated as insulating. The metallic surface character of the reconstructed basal plane of α-Al_2O_3 may present interesting implications for future applications of heat-treated alumina surfaces.

I. Introduction

Alumina, Al_2O_3, is a material encountered in engineering applications as a commonly used ceramic, as well as appearing as a self-limiting oxide layer on aluminum and its alloys. More recently, it has received considerable interest due to an array of potential uses related to electronics, as a possible replacement gate oxide material. A variety of electronics applications focus on properties associated with growth of ultrathin metal films, e.g. Cu, on an alumina substrate.[1−4]

The most stable, well-characterized phase of alumina is α-Al_2O_3. A preferred surface for alumina substrates is its basal plane, of which there are two commonly studied, stable terminations: the α-Al_2O_3(0001)-(1 × 1) surface and its ($\sqrt{31} \times \sqrt{31}$)$R \pm 9°$ reconstruction. Although there have been numerous semiempirical and ab initio studies of the (1 × 1) termination, the size of the ($\sqrt{31} \times \sqrt{31}$)$R \pm 9°$ reconstructed surface has prohibited any ab initio investigations, instead limiting the few studies that have attempted to explore this surface to structure optimizations using empirical potentials.[5,6]

The hexagonal cell of α-Al_2O_3 contains six Al_2O_3 units with a stacking Al−O_3–Al−Al−O_3–Al−Al−O_3–Al− ···. A picture of this hexagonal cell is shown in Figure 1. Although this structure presents several cleavage-site options, the preferred cut for the basal plane cleavage site is between the Al layers such that stoichiometric surface structures can be obtained with minimal bond breaking (and breaking only the weakest bonds). This cleavage plane is indicated in Figure 1. Details of the (1 × 1) surface termination are quite controversial. Some studies suggest an oxygen-terminated surface,[7] and others determine that the surface may be composed of mixed oxygen and aluminum domains,[8−10] while considerable recent evidence indicates that a surface terminated with a single layer of aluminum is the most likely candidate.[11−13] This single Al-layer termination is also found to be most favorable in theoretical predictions.[14] Some of the apparent confusion with respect to surface termination is likely due to the large inward relaxations

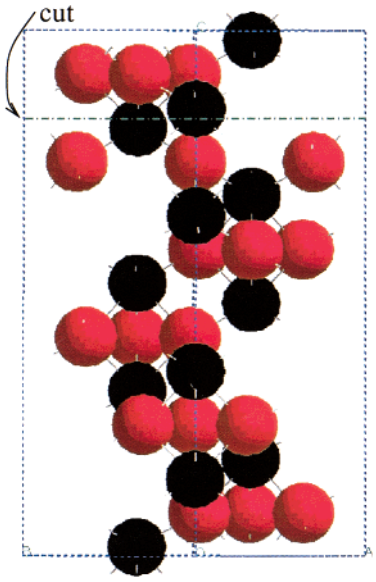

Figure 1. Hexagonal unit cell of α-alumina showing preferred basal plane cut between the aluminum layers. The black spheres are aluminum, and the red ones are oxygen.

† Part of the special issue "John T. Yates, Jr., Festschrift".

* To whom correspondence should be addressed. Fax: (310)267-0319. E-mail: eac@chem.ucla.edu.

10.1021/jp003587c CCC: $20.00
Published on Web 02/17/2001

of the surface aluminum atoms such that the underlying oxygen plane is very near the surface.

Experimental characterization of the energetics and surface structure of the (1×1) termination of the (0001) plane of α-Al_2O_3 is somewhat complicated. Creating the Al-terminated surface by fracture using the double-cantilever-cleavage technique is difficult or impossible.[15] However, as mentioned earlier, the (0001) surface can grow in during Al_2O_3 formation via aluminum oxidation.[16] In section IIIA, we discuss specifics of the energetics and atomic relaxations calculated for this surface.

As already mentioned, another stable (0001) surface termination is the $(\sqrt{31} \times \sqrt{31})R \pm 9°$ reconstruction. Controversy also exists regarding the experimentally determined $(\sqrt{31} \times \sqrt{31})R \pm 9°$ termination. In fact, this reconstruction is sufficiently complicated and dependent on sample preparation so as to warrant the inclusion of α-Al_2O_3(0001) in a 1997 article by Chame et al. entitled "Three Mysteries of Surface Science".[6] Although progress has been made on understanding some aspects of this reconstruction,[5,7,18−21] a major question, namely certain details of the electronic structure for this surface, has been left largely unanswered. Specifically, evidence for the anticipated metallic nature of an aluminum-enriched surface[6] has been lacking, conflicting, or ignored. In this paper, we investigate a model $(\sqrt{31} \times \sqrt{31})R \pm 9°$ surface and compare it with the stoichiometric (1×1) termination. Our analyses show strong evidence of metallic surface states.

The $(\sqrt{31} \times \sqrt{31})R \pm 9°$ reconstruction of alumina (0001) can be obtained by heating under vacuum. In fact, this structure is the final stage in a series of reconstructions: $(1 \times 1) \rightarrow (2 \times 2) \rightarrow (3\sqrt{3} \times 3\sqrt{3})R30° \rightarrow (\sqrt{31} \times \sqrt{31})R \pm 9°$,[22] where the surface structure designations (e.g. $3\sqrt{3} \times 3\sqrt{3}$) are defined by coefficients of the matrixes that transform between bulk unit cell vectors and those of the reconstructed surface. In the $(\sqrt{31} \times \sqrt{31})R \pm 9°$ reconstruction, matrixes **A** and **B** generate the vectors of the surface domains consistent with the resulting diffraction patterns,

$$\mathbf{A} = \begin{pmatrix} 11/2 & \sqrt{3/2} \\ -\sqrt{3/2} & 11/2 \end{pmatrix} \quad \mathbf{B} = \begin{pmatrix} 11/2 & -\sqrt{3/2} \\ \sqrt{3/2} & 11/2 \end{pmatrix}$$

and the $(\sqrt{31} \times \sqrt{31})R \pm 9°$ designation refers to the fact that the new unit vectors of the surface are expanded by $\sqrt{31}$ and the surface cell is rotated by $\pm 9°$ from the original (1×1).[18] Although the common preparation method for the $(\sqrt{31} \times \sqrt{31})R \pm 9°$ relies on high-temperature annealing in UHV, low energy electron diffraction (LEED) of room-temperature aluminum deposition on an (0001) Al_2O_3 (1×1) substrate also display the characteristic $(\sqrt{31} \times \sqrt{31})R \pm 9°$ pattern at low coverages (less than 5 monolayers) of Al.[17]

It has been understood for many years that the $(\sqrt{31} \times \sqrt{31})R \pm 9°$ surface contains reduced aluminum. An early experimental study of the (0001) surface reconstruction speculated that the alumina surface was in a reduced valence state, since oxygen evaporation was detected by mass spectrometry. The LEED pattern was consistent with a surface composed of a cubic layer over the hexagonal lattice of stoichiometric alumina.[18] This overlayer was postulated to consist of a nominally fluorite or fcc structure with Al_2O or AlO chemical composition, respectively. Angle-resolved X-ray photoelectron spectroscopy (XPS) data showed relative concentrations of Al and O to be consistent with an AlO surface composition, although evidence of a reduced aluminum species was not detected.[7] However, later XPS data by Gautier et al. display a small reduced aluminum component, corresponding to the aluminum metallic state; furthermore, this same study showed electron energy loss spectroscopy (EELS) evidence for metallic states of the reconstructed alumina surface.[22]

Several years later, it was shown that the hypothesis of a reduced cubic overlayer on the hexagonal alumina sublattice as the atomic structure of the $(\sqrt{31} \times \sqrt{31})R \pm 9°$ surface was inconsistent with more recent experimental observations. In 1994, Gautier et al. reported the atomic structure of the $(\sqrt{31} \times \sqrt{31})R \pm 9°$ termination corresponded to two planes of aluminum in a structure similar to fcc aluminum (111), based on grazing incidence X-ray scattering and LEED data.[5] Similar findings were also reported by Renaud et al.[21] These authors suggested that the reconstructed surface was achieved after the two outermost oxygen planes of the (1×1) surface had been evaporated. Auger spectroscopy and LEED of Al deposition on alumina (0001) by Vermeersch et al. further supported this new description of the reconstructed surface structure.[19] The previous data, which had led to speculation of a cubic overlayer, did not contradict this newly proposed structure. It seems that an "Al(111)" termination of the alumina $(\sqrt{31} \times \sqrt{31})R \pm 9°$ surface, formed by evaporation of the two outermost oxygen layers (or alternatively by aluminum deposition), is now the generally accepted surface structure for this reconstruction.[6]

II. Calculational Details

We performed calculations within the generalized gradient approximation (GGA-PW91)[23] to density functional theory (DFT)[24] using the Vienna Ab Initio Simulation Package (VASP).[25] These calculations employed periodic boundary conditions, expanded the valence electron density in a plane-wave basis, and replaced the core electrons with ultrasoft pseudopotentials.[26] Nonlinear core corrections to the exchange-correlation were included for Al. Dipole corrections perpendicular to the surfaces were calculated for all structures and found to be negligibly small, having an effect of less than 0.01 eV on the total energy in every case.

For bulk alumina, we tested for convergence of the **k**-point sampling density and kinetic energy cutoff. A kinetic energy cutoff of our plane-wave basis of 340 and 560 eV for the representation of the augmentation charges, necessary since the ultrasoft pseudopotentials are not norm-conserving, was found to yield total energies converged to within the meV/atom range. A Monkhorst−Pack grid was used for the Brillouin zone integration. A Monkhorst−Pack grid of $3 \times 3 \times 1$, i.e., 5 **k**-points in the irreducible Brillouin zone of our hexagonal alumina cell, was employed for our bulk calculations. We uniformly scaled the lattice vectors and performed single-point energy calculations to sample a region within ~5% of the equilibrium volume. These data was then fit to Murnaghan's equation of state[27]

$$E(V) = \frac{B_o V}{B_o'}\left[\frac{\left(\frac{V_o}{V}\right)^{B_o'}}{B_o' - 1} + 1\right] + C \qquad (1)$$

(with $E(V)$ the total energy, V the volume, V_o the equilibrium volume, B_o the bulk modulus with pressure derivative B_o', and C a constant). We obtained a bulk modulus with <10% deviation from experiment and an equilibrium volume within 3% of the experimentally determined value.[28]

For the surface calculations, we converged the total energies with respect to slab and vacuum thickness and atomic relax-

ations. As mentioned earlier, the alumina (0001) surface presents several cleavage plane options. In our calculations, we imposed the constraint of having stoichiometric alumina slabs with equivalent faces. This allowed two possibilities: a single Al-layer termination or an O-layer termination with half of the oxygen atoms removed on either side of a cell doubled in the slab plane. Preliminary studies showed the oxygen-terminated surfaces to be much less energetically favorable, having surface energies nearly twice those of the Al-terminated surface. Other possible cleavage sites of the (1×1) α-Al_2O_3 surface have been studied previously and also found to be less stable.[14] These findings, and the experimental evidence suggesting the single Al-layer termination,[11] led us to focus solely on the Al-termination of the (1×1) surface for the remainder of the study.

Although the (1×1) termination only required 5 **k**-points in the irreducible Brillouin zone, the possible metallic nature of the Al-rich terminations required a higher number of **k**-points to properly characterize. Using 13 **k**-points in the irreducible Brillouin zone resulted in total energies converged within 0.01 eV/atom compared to those using twice that number of **k**-points; for consistency, we used this higher (13) **k**-point sampling density for the stoichiometric and Al-rich surface calculations. We performed calculations using the Methfessel−Paxton[29] Fermi surface smearing method with a smearing width of 0.1 eV, as well as using Blöchl's corrected version of the tetrahedron integration method.[30] Both techniques yielded very similar total energies, within 1 meV/atom; the total entropy term introduced by the Methfessel−Paxton smearing was less than 0.01 eV.

The full periodic cell of the $(\sqrt{31} \times \sqrt{31})R \pm 9°$ reconstruction was not feasible to simulate within our DFT study. Instead, we simulated a model with the same lattice vectors as the (1×1) termination cell, i.e., the bulk alumina lattice vectors in the surface plane. As mentioned earlier, the $(\sqrt{31} \times \sqrt{31})R \pm 9°$ reconstruction is thought to correspond to removal of the two outermost oxygen layers accompanied by a corresponding rearrangement of the surface aluminum atoms.[21] The transition to the Al-rich reconstructed surface was simulated by annealing and quenching two structures. One of these structures was formed by removal of a single oxygen layer, and the other structure had two oxygen layers removed, on each surface. This second structure is the one postulated to correspond to the reconstructed surface termination, without the additional rotation/expansion of the $(\sqrt{31} \times \sqrt{31})R \pm 9°$ surface lattice vectors. The annealing of these surfaces was performed at a temperature above which the $(\sqrt{31} \times \sqrt{31})R \pm 9°$ reconstruction takes place. We found the atomic relaxations and surface energy of the basal (1×1) surface to be well-converged using a slab thickness of 4 Al_2O_3 units, 8.25 Å. As a result, we created our initial (1×1) surface to be 8 Al_2O_3 units thick and then removed the outer oxygen planes to create the Al-rich surfaces. Accordingly, the "$(\sqrt{31} \times \sqrt{31})R \pm 9°$" surface still maintained 4 stoichiometric alumina layers at its center. The annealing was performed via DFT molecular dynamics simulating a canonical ensemble at a temperature of 1700 K using a Nosé thermostat with a frequency of 70 THz.[31] This frequency was chosen based on vibrational frequencies (phonons) of alumina thin films.[32] The trajectory lengths were up to 0.7 ps using a time step of 0.40 fs. The structures obtained from these dynamics were subsequently quenched to their equilibrium structures so that the forces on all atoms were less than 0.05 eV/Å.

III. Results

A. Al_2O_3(0001) Surfaces. Our findings of the Al-terminated Al_2O_3(0001) surface as the most stable is consistent with similar predictions from DFT embedded cluster calculations.[14] A recent DFT study by Wander et al. found that the specific choice of exchange-correlation functional has some effect on the predicted surface structure.[33] Likewise, although all theory does predict large inward relaxations of the surface aluminum, the extent of these relaxations does depend somewhat on the theoretical model employed.[34] Since alumina is a highly ionic material, the bulk-like surface termination is unfavorable since it leaves a "bare" surface $Al^{\sim 3+}$; thus, a large inward relaxation of this surface aluminum results in a more energetically favorable structure whereby the oxygen anions can more effectively screen the positive charge of the aluminum. We found large inward relaxation of the surface aluminum atoms in all cases, as has been reported previously.[35−39] DFT-GGA predicts the bulk Al−O bond length to be 1.87 Å, which decreases to 1.67 Å for the surface Al−O bonds upon relaxation. This decrease in bond length is associated with a 0.73 Å vertical relaxation of the unit cell's surface aluminum atoms (one on each side of the slab), concurrent with horizontal expansion of the three oxygen atoms in the surface O-planes. The unit cell vectors were fixed at DFT-GGA bulk values throughout the calculation to represent a semi-infinite crystal; only the relative atomic positions were allowed to change. Previous studies that allowed only relaxation of the interlayer spacing, and not of the individual atomic coordinates, could not include this effect.[36,40] More recent studies investigating Al_2O_3(0001), using Hartree−Fock and LDA calculations, have reported geometrical relaxations for 9- and 18-layer slabs but did not calculate surface energies.[41,42] LDA calculations by Verdozzi et al.,[42] for a surface with a thickness of 18 Al_2O_3 units, showed similar (within 0.02 Å) vertical relaxations of the three outermost atomic layers compared to our calculations that used a thickness of only 4 Al_2O_3 units. Furthermore, our calculated surface energies for 4 and 5 Al_2O_3 unit layer thicknesses differed by only 0.1%, well within the error of our calculations. Accordingly, we are confident that a thickness of 4 stoichiometric alumina layers maintained in our most Al-rich surfaces is sufficiently thick to ensure that both sides of the slab behave as isolated surfaces.

Below ~1220 K, it is difficult to experimentally obtain reliable surface energies of clean Al_2O_3 due to hydroxylation. An empirical expression for the experimental surface energy of the alumina (0001) surface is 892 (ergs/cm^2) − 0.12T (°C) obtained by using values of the surface energy at 1363 and 4660 °C and assuming a constant coefficient in this temperature range.[43] The reliability of such an estimate over the temperature range is not possible to ascertain with only two data points, and its validity in extrapolation to much lower temperatures might also be suspect. Nevertheless, assuming that a constant coefficient is a reasonable approximation, the experimental estimate of 925 mJ/m^2 for the (0001) plane of α-Al_2O_3 at zero temperature is well below any theoretically predicted value. We obtain a surface energy of just under 1500 mJ/m^2 for the (1×1) surface termination. Previous estimates of this surface energy using empirical potentials have reported values above 2000 mJ/m^2.[35,38,39] Since such potentials generally are not fit to surface energies, these estimates are likely to be inaccurate. Hartree−Fock and density functional studies employing the local density approximation (LDA) also obtained higher surface energies, with the Hartree−Fock calculations yielding a surface energy of nearly 4000 mJ/m^2 [37] and the LDA predicting surface energies near 1800 mJ/m^2.[36] As Hartree−Fock is well-known

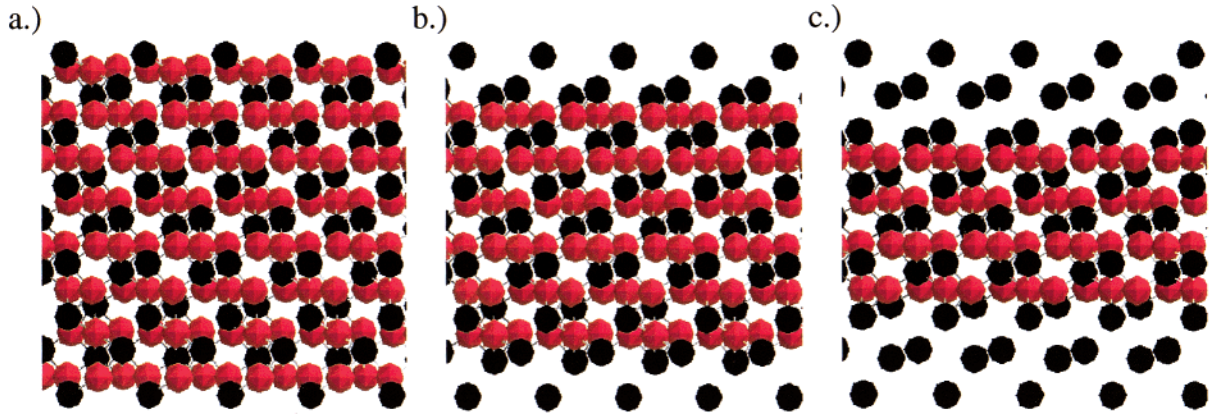

Figure 2. Unrelaxed structures of (a) stoichiometric, (b) one oxygen layer removed, and (c) two oxygen layers removed Al_2O_3(0001) surfaces.

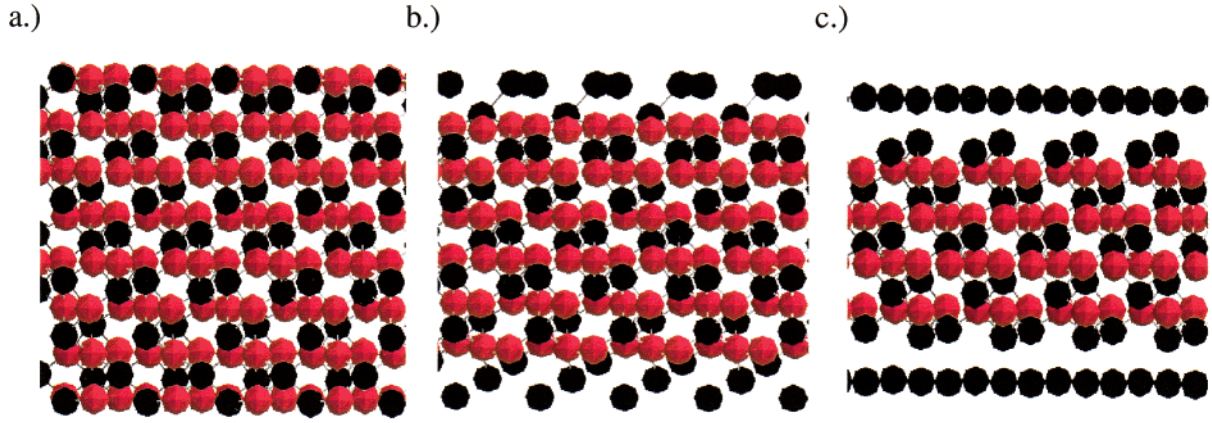

Figure 3. Relaxed structures of (a) stoichiometric, (b) one oxygen layer removed, and (c) two oxygen layers removed Al_2O_3(0001) surfaces.

not to describe bond breaking correctly and since DFT-LDA is well-known for its tendency to overbind, it is not surprising that these predictions are significantly higher than our prediction here. The DFT-GGA prediction may also be slightly high, but it is the best estimate available with current theoretical techniques. Unlike the large discrepancy in predicted surface energies, all methods find that surface relaxations have a large impact on surface energy. The relaxed surface energies in each calculation (with the exception of Hartree−Fock[37]) are less than 50% of the surface energy obtained with bulk termination.

B. (1 × 1) to ($\sqrt{31} \times \sqrt{31}$)*R*±*9*° *Reconstruction.* Figure 2 displays the unrelaxed atomic positions for the three surfaces investigated in our study, and Figure 3 displays these same views after annealing/quenching. The large inward relaxations of the surface aluminum in the (1 × 1) termination are apparent in Figure 3a. Likewise, the rearrangement of the aluminum surface layer in the ($\sqrt{31} \times \sqrt{31}$)$R \pm 9°$ reconstructed surface is also worthy of note. The atomic arrangement of the outermost aluminum surface plane has been described as resembling a layer of fcc (111) aluminum, based on grazing incidence X-ray diffraction.[21] As can be seen in Figure 4, our predicted structure for this outermost aluminum plane after annealing/quenching is very similar to an ideal (111) aluminum plane, in agreement with the structure inferred from experiment. The distance between aluminum nearest-neighbors in the DFT-GGA-predicted ($\sqrt{31} \times \sqrt{31}$)$R \pm 9°$ reconstructed surface is 2.80 Å, compared with a bulk fcc aluminum DFT-GGA nearest-neighbor distance of 2.86 Å. This 2% contraction relative to bulk aluminum occurs in our simulation since the full surface reconstruction is not allowed to take place; we are not allowing a change in the unit cell vectors to accompany the atomic rearrangements. Nevertheless, as shown in Figure 4, our reconstructed surface does display the desired Al(111) fcc surface structure.

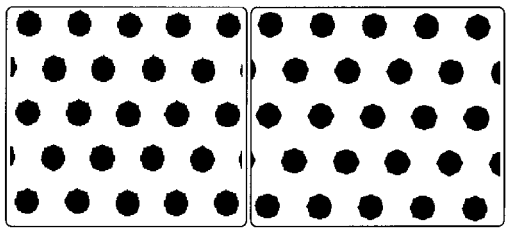

Figure 4. Top view of ($\sqrt{31} \times \sqrt{31}$)$R \pm 9°$ surface plane and an aluminum (111) surface. The nearest-neighbor distances are 2% smaller in the ($\sqrt{31} \times \sqrt{31}$)$R \pm 9°$ surface since the lattice vector lengths are those of the DFT-GGA bulk Al_2O_3 substrate.

The structure formed upon partial reduction of the surface is shown in Figure 3b. The relaxed atomic coordinates for this surface with one oxygen layer removed slowly converged to inequivalent atomic positions of the outermost surface aluminum atoms. The structure shown corresponds to a local minimum. Tests calculations, creating equivalent surfaces on both sides of the alumina slab without allowing relaxations, showed that the two inequivalent positions were very similar in energy (a difference of only 0.1% in the total cohesive energy of the two structures).

Figure 5 displays a cross-sectional valence electron density cut through the relaxed alumina surface slabs shown Figure 3, first for the stoichiometric (1 × 1) slab, then for the case with removal of a single surface oxygen layer, and finally with

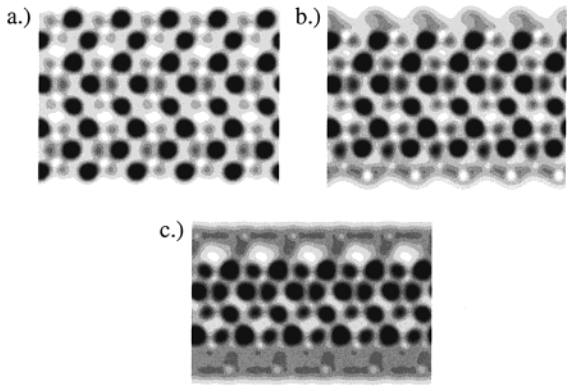

Figure 5. Vertical cut through valence electron density of the (relaxed) stoichiometric and Al-rich terminations of alumina where (a) is (1 × 1) stoichiometric, (b) has one oxygen layer removed, and (c) has two oxygen layers removed on each side of the slab. There are 10 contours spanning a range of 0−1. The dark areas are where the oxygen anions reside.

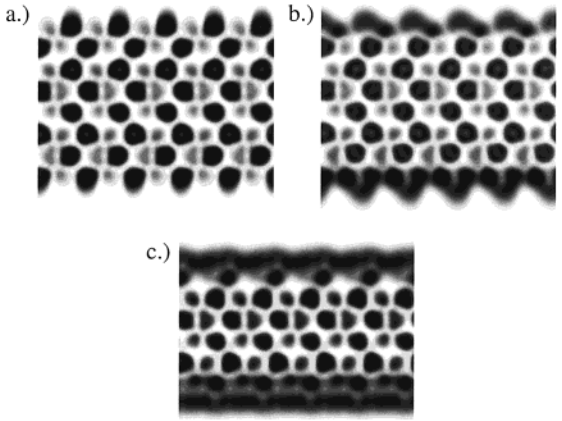

Figure 6. Vertical cut through the "ELF" values for the valence electron density of the relaxed structures corresponding to Figure 5a−c. The contours are divided by intervals of 0.1, with the maximum value shown being 0.9 (darkest).

removal of the two surface oxygen layers to create the "$(\sqrt{31} \times \sqrt{31})R \pm 9°$" termination. It is apparent that the Al-rich terminations exhibit very different behavior of the surface density from that of the stoichiometric alumina. In the stoichiometric, ionic slab, the density is highly localized around the negatively charged oxygen atoms and the aluminum positions are not visible. With aluminum enrichment at the surface, the valence electron density in that region becomes much more uniform (see Figure 5b,c).

Perhaps a more informative plot related to Figure 5 is shown in Figure 6. This figure shows the cross-sectional electron localization function (ELF) values for the valence electron density of the three alumina slabs. The ELF is designed to provide insight into the nature of bonding in molecules and crystal structures by providing a measure of the "degree of localization" of the electrons via analysis based on the Pauli principle.[44] The mathematical description of the ELF is

$$\mathrm{ELF}(\mathbf{r}) = \frac{1}{1 + \left[\frac{D(\mathbf{r})}{D_h(\mathbf{r})}\right]^2} \qquad (2)$$

where $D(\boldsymbol{r})$ is the Pauli excess kinetic energy density and $D_h(\boldsymbol{r})$ is the kinetic energy of the homogeneous electron gas for a density equal to the local density.[45] [Note: $D(\boldsymbol{r}) = T + T_{corr} - T_{Bose}$, where T is the kinetic energy of the noninteracting Kohn−Sham system ($-2\frac{\hbar^2}{2m}\sum_i \phi_i^* \nabla^2 \phi_i$), the kinetic energy "correlation" correction component is $T_{corr} = (1/2)(\hbar^2/2m)\nabla^2\rho$ to ensure $T + T_{corr}$ is positive definite, and T_{Bose} is the ideal Bose gas kinetic energy ($(1/4)(\hbar^2/2m)(|\nabla\rho|^2/\rho)$).] The ELF value is 0.5 for a homogeneous electron gas and can increase to ∼1.0 for electrons paired in a covalent bond or a highly localized, unpaired electron in a dangling bond.

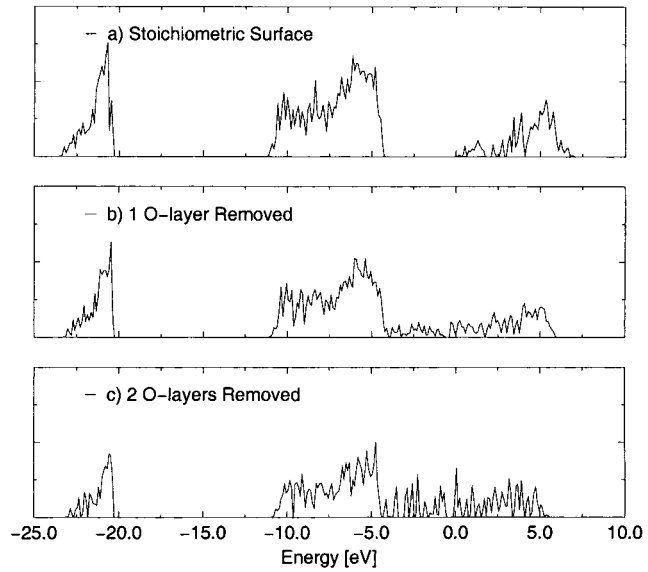

Figure 7. Density of states (DOS) plots for the stoichiometric and Al-rich terminations of $Al_2O_3(0001)$. The stoichiometric surface corresponds to the (1 × 1) termination, and the removal of 2 oxygen layers is our "$(\sqrt{31} \times \sqrt{31})R \pm 9°$" reconstruction model.

The ELF values for our $(\sqrt{31} \times \sqrt{31})R \pm 9°$ reconstruction were extremely interesting. A recent study by De Santis and Resta characterized three low-index surfaces of aluminum using the ELF.[46] For the (111) surface, they found that, in the surface plane, the ELF values were very uniform at a value near 0.5, i.e., metallic bonding. Furthermore, they found that the highest ELF value for this surface occurred slightly off the terminating plane of aluminum, in the vacuum region, and reached a maximum of 0.73. As in the Al(111) surface, the terminating plane of our $(\sqrt{31} \times \sqrt{31})R \pm 9°$ reconstructed surface is predicted to be composed of aluminum atoms arranged with six in-plane nearest neighbors, as shown in Figure 4. Interestingly, we find remarkably similar behavior of the ELF for this plane of atoms as that described for the (111) surface of the much thicker slab of aluminum, i.e., near-uniform metallic ELF values in the plane and a maximum, occurring somewhat beyond this plane, that reaches values of 0.72−0.75. Conversely, the bonding between this outermost "Al(111)" plane and the aluminum in the outermost layer(s) associated with the stoichiometric Al_2O_3 showed more localized interactions, with ELF values above 0.8 between these aluminum atoms. The ELF plots for the (1 × 1) termination and the surface created by removal of a single oxygen layer are perhaps less surprising. The (1 × 1) termination shows electron density localized on the oxygen ions for both surface and bulk-like states. The termination resulting from removal of the single oxygen layer shows the more localized interactions between aluminum atoms at the surface similar to those between the outermost aluminum plane and the deeper aluminum associated with the oxygen plane in the reconstructed surface.

The total density of states (DOS) for the stoichiometric and oxygen-deficient alumina slabs are shown in Figure 7. The zero

of energy is the Fermi level for the "$(\sqrt{31} \times \sqrt{31})R \pm 9°$" termination. The DOS are aligned according to the top of the O 2*s* band for the three structures, which is the lowest energy band shown. Note the band gap in the DOS plot for the stoichiometric (1×1) surface structure (Figure 7a). As can be seen from this figure, the metallic characteristics of the DOS (i.e., states at the Fermi level, no band gap) grow in with Al-enriched surfaces. For the "$(\sqrt{31} \times \sqrt{31})R \pm 9°$" termination, the metallic nature of the DOS is strongly apparent.

The electron density associated with each individual atom in a binary system is difficult or impossible to define in a quantitative manner; selecting a radius for the projected local DOS, etc., is somewhat ambiguous. However, it is possible to analyze the density such that trends, qualitative behavior, and even quantitative comparisons to similar systems can be determined. In our choice of atomic radii, we attempted to minimize overlap between spheres defining the local atomic radii, while at the same time maximizing the density accounted for within these atomic spheres. Radii of 1.015 and 1.345 Å for aluminum and oxygen, respectively, resulted in ~1.25 interstitial e^-/Al_2O_3 unit (i.e., not contained within the atomic spheres). For consistency, we used these radii for the three surfaces, although naturally the delocalized electron density of the metallic aluminum resulted in significantly more electron density in the interstitial region. For the most Al-rich termination, considerable valence electron density, ~2 e^-/surface Al, was in the interstitial region. We found the occupations to be nearly identical, within 0.01 e^-, when comparing the local occupations for our $(\sqrt{31} \times \sqrt{31})R \pm 9°$ surface Al atoms to those of bulk aluminum using the same radius. Using a larger radius of 1.4 Å for aluminum and comparing the occupations of the surface aluminum in our $(\sqrt{31} \times \sqrt{31})R \pm 9°$ termination to those of bulk aluminum showed a difference of only 2% for the aluminum occupations in these two environments. This larger radius resulted in only 1.2 e^-/Al atom in the interstitial region. Our local DOS analysis is supportive of the additional electrons in the reduced surface being isolated to the region of the aluminum overlayer. The chosen radii for oxygen and aluminum capture 95% of the valence electron density in the stoichiometric structure; i.e., only 5% of the valence electron density is in the interstitial region not associated with any of the atomic spheres. The charges on the aluminum and oxygen ions in the deeper region of the reduced structure, namely, those below the aluminum overlayer, are identical to within ~0.01 e^-/atom to those of the subsurface ions in the stoichiometric structure. However, for the reduced surface, there are additional electrons not associated with ionic spheres. This can be seen in Figure 5 as a gray band appearing at the top and bottom of the alumina slab, corresponding to the location of the aluminum surface layers. As mentioned, the valence electron density associated with the Al surface ions is effectively identical to the values found in bulk aluminum. Although certain oxygen positions appear darker in Figure 5c than in Figure 5a, this is not a consequence of actual charge increase in a 3D projection sphere around those ions; rather it results from a slight difference in ionic coordinates relative to the vertical electron density slice displayed.

Figure 8 shows the projected local DOS for surface Al atoms in the stoichiometric and Al-enriched surfaces. The change from insulating to metallic character with increasing deviation from Al_2O_3 stoichiometry is strongly apparent. Conversely, Figure 9 displays a similar plot, this time for an Al atom near the center of the alumina slab. These are similar in all cases, with the occupied states being nearly identical. Thus the increasing metallic character with oxygen depletion at the surface does not affect the electronic structure of the subsurface layers of Al_2O_3.

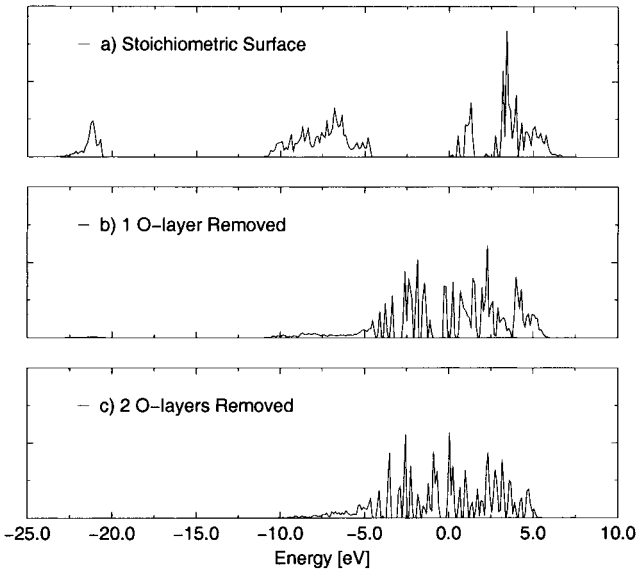

Figure 8. Projected local density of states (LDOS) for a surface Al atom for the three structures. The energies are aligned in the same manner as described in Figure 7.

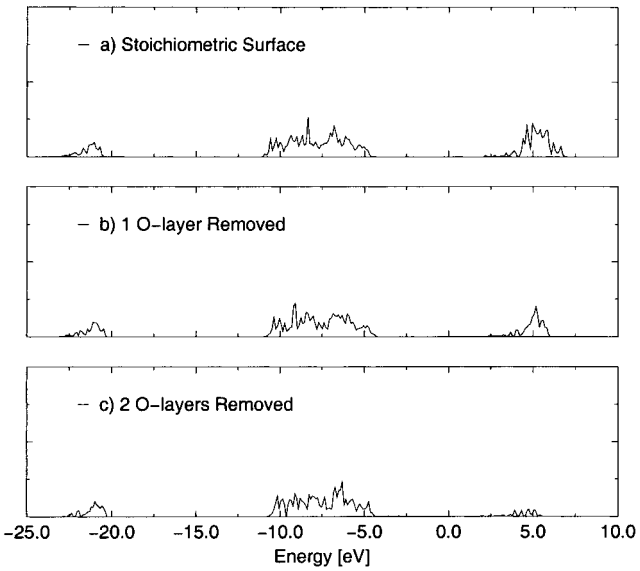

Figure 9. Projected local density of states (LDOS) for an Al atom in the center of the alumina slab, i.e., a "bulk-like" atom, for the three surface structures. The energies are aligned in the same manner as described in Figure 7.

We observed a slight decrease, less than 0.1 e^-, in the charge of the oxygen layer nearest to the surface in the $(\sqrt{31} \times \sqrt{31})R \pm 9°$ reconstructed surface compared with the (1×1) termination. In fact, the charges on these oxygen ions in the reconstructed surface corresponded to those of subsurface oxygen ions in the (1×1) termination as previously discussed. This decrease in the charge on the oxygen layer nearest to the surface for the reconstructed termination was suggested by Gautier et al. upon detailed study of the Auger O *KLL* line shape of the XPS spectrum.[5] EELS in this paper indicate a ~1 eV decrease in band gap between this surface and the (1×1) surface; however, there is no noticeable metallic character to the reconstructed surface in these spectra. Likewise, valence band photoemission spectra of the surfaces in this study are

consistent with the EELS spectra; namely, they do not show a metallic peak. By contrast, earlier EELS spectra by Gautier et al. do show evidence of surface metallic states.[22] Unfortunately, valence band photoemission spectra were not reported in this earlier study showing evidence of metallic states. The apparent discrepancy in the EELS spectra was not discussed, and the later paper makes no reference to metallic states. Nevertheless, it is interesting to note this early indication of experimental evidence for surface metallic states. As mentioned earlier, subsequent experiments seem to ignore or not observe such features.

IV. Conclusions

The lack of conclusive experimental evidence for the metallic nature of the $(\sqrt{31} \times \sqrt{31})R \pm 9°$ Al_2O_3 surface reconstruction is intriguing and somewhat surprising considering that this is a widely studied surface. We find strong evidence for the appearance of metallic surface states in our DFT study of the (1×1) to $(\sqrt{31} \times \sqrt{31})R \pm 9°$ transition. Although we are unable to simulate the full unit cell of the reconstructed surface, the relative atomic arrangements at our surface are quite similar to those described for the true structure.

XPS measurements show the band gap for (0001) alumina (1×1) to be $\sim 8-8.5$ eV.[5,47] However, semiempirical theory and experimental evidence predict the existence of surface state bands within this gap.[20,48] Although our calculations underestimate the band gap, qualitative information can be obtained by density of states (DOS) analysis. [Note: Our calculated band gap is only 5 eV when surface states are included. However, for the interior of the alumina slab, DOS values ≥ 0.05 result in a band gap of 8 eV.] This information, along with analysis of the valence density, the ELF, and the $(\sqrt{31} \times \sqrt{31})R \pm 9°$ surface structure plots, indicates that the decrease in band gap associated with the reconstruction is much more dramatic than has been stressed in the literature (where there are references to a decrease of only 1 eV, resulting in a band gap of 7 eV, for this termination).[5] Both the (1×1) and the $(\sqrt{31} \times \sqrt{31})R \pm 9°$ termination are commonly discussed as being insulating surfaces, even in recent articles.[4,5] As mentioned earlier, Chame et al. anticipate the presence of metallic states, and (somewhat inconclusive) XPS and EELS evidence[22] suggests that such states are present. We say "inconclusive" since similar spectra do not clearly show such features.[5,7]

Although our $(\sqrt{31} \times \sqrt{31})R \pm 9°$ surface model does not incorporate the true lattice vectors of the reconstructed alumina surface, the relative atomic arrangements of the aluminum atoms in our reconstructed surface are consistent with the reported Al-(111)-like surface structure.[21] Accordingly, we expect our analysis to provide a good qualitative description of the true $(\sqrt{31} \times \sqrt{31})R \pm 9°$ surface. As such, we find the possible surface metallic states, predicted in our calculations, warrant further experimental investigation. It would be interesting to determine if highly sensitive STM studies could be performed on this reconstructed surface. Likewise, it would be interesting to note if ultraviolet photoelectron spectroscopy and/or metastable He de-excitation spectroscopy could display the metallic feature. To our knowledge, no such spectra have been obtained for this reconstructed surface (except for the photoemission spectra by Gautier et al.[5] which did not show this feature.) Obtaining a more complete understanding of such metallic states could be of paramount importance, for instance, in the behavior of interfaces in gate oxides, where maintaining an effective high dielectric constant is critical. If such metallic behavior were to exist at these interfaces, dielectric breakdown could be expected.

Acknowledgment. We are grateful to the Air Force Office of Scientific Research for personnel funding. This research, in part conducted at the Maui High Performance Computing Center, was sponsored in part by the Air Force Research Laboratory, Air Force Materiel Command, USAF, under cooperative agreement No. F29601-93-2-0001. The views and conclusions contained in this document are those of the author(s) and should not be interpreted as necessarily representing the official policies or endorsements, either expressed or implied, of the Air Force Research Laboratory, the U.S. Government, The University of New Mexico, or the Maui High Performance Computing Center.

References and Notes

(1) Gautier, M.; Duraud, J. P.; Pham Van, L. *Surf. Sci. Lett.* **1991**, *249*, L327.
(2) Gota, S.; Gautier, M.; Douillard, L.; Duraud, J. P.; Le Fevre, P. *Surf. Sci.* **1995**, *323*, 163.
(3) Gota, S.; Gautier-Soyer, M.; Douillard, L.; Duraud, J. P.; Le Fevre, P. *Surf. Sci.* **1996**, *352*−*354*, 1016.
(4) Pang, C. L.; Raza, H.; Haycock, S. A.; Thornton, G. *Surf. Sci.* **2000**, *460*, L510.
(5) Gautier, M.; Renaud, G.; Pham Van, L.; Villette, B.; Pollak, M.; Thromat, N.; Jollet, F.; Duraud, J.-P. *J. Am. Ceram. Soc.* **1994**, *77*, 323.
(6) Chame, A.; Lançon, F.; Paliti, P.; Renaud, G.; Vilfan, I.; Villain, J. *Int. J. Mod. Phys. B* **1997**, *11*, 3657.
(7) Arbab, M.; Chottiner, G. S.; Hoffman, R. W. *Mater. Res. Soc. Symp. Proc.* **1989**, *153*, 63.
(8) Guglielmacci, J.-M.; Ealet, B. *Mater. Sci. Eng. B* **1996**, *40*, 96.
(9) Heffelfinger, J. R.; Bench, M. W.; Carter, C. B. *Surf. Sci.* **1997**, *370*, L168.
(10) Toofan, J.; Watson, P. R. *Surf. Sci.* **1998**, *401*, 162.
(11) Guénard, P.; Renaud, G.; Barbier, A.; Gautier-Soyer, M. *Surf. Rev. Lett.* **1997**, *5*, 321.
(12) Ahn, J.; Rabalais, J. W. *Surf. Sci.* **1997**, *388*, 121.
(13) Suzuki, T.; Hishita, S.; Oyoshi, K.; Souda, R. *Surf. Sci.* **1999**, *437*, 289.
(14) Guo, J.; Ellis, D. E.; Lam, D. J. *Phys. Rev. B* **1992**, *45*, 13647.
(15) Wiederhorn, S. M. *J. Am. Ceram. Soc.* **1969**, *52*, 485.
(16) Clausen, E. M.; Hren, J. J., Jr. The Gamma to Alpha Transformation in Thin Film Alumina. *Mater. Res. Soc. Symp. Proc.* **1985**, *41*, 381.
(17) Vermeersch, M.; Sporken, R.; Lambin, Ph.; Caudano, R. *Surf. Sci.* **1990**, *235*, 5.
(18) French, T. M.; Somorjai, G. A. *J. Phys. Chem.* **1970**, *74*, 2489.
(19) Vermeersch, M.; Malengreau, F.; Sporken, R.; Caudano, R. *Surf. Sci.* **1995**, *323*, 175.
(20) Gillet, E.; Ealet, B. *Surf. Sci.* **1992**, *273*, 427.
(21) Renaud, G.; Villette, B.; Vilfan, I.; Bourret, A. *Phys. Rev. Lett.* **1994**, *73*, 1825.
(22) Gautier, M.; Duraud, J.-P.; Pham Van, L.; Guittet, M. J. *Surf. Sci.* **1991**, *250*, 71.
(23) Perdew, J. P. *Phys. Rev. B* **1986**, *33*, 8822; **1986**, *34*, 7406 (E). Perdew, J. P.; Wang, Y. *Phys. Rev. B* **1992**, *45*, 13244.
(24) Hohenberg, P.; Kohn, W. *Phys. Rev. B* **1964**, *136*, 864. Kohn, W.; Sham, L. J. *Phys. Rev A* **1965**, *140*, 1133.
(25) Kresse, G.; Haffner, J. *Phys. Rev B* **1993**, *47*, 558; **1994**, *49*, 14251. Kresse, G.; Furthmuller, J. *Comput. Mater. Sci.* **1996**, *6*, 15.
(26) Vanderbilt, D. *Phys. Rev. B* **1990**, *41*, 7892. Kresse, G.; Hafner, J. *J. Phys.: Condens. Matter* **1994**, *6*, 8245.
(27) Murnaghan, F. D. *Proc. Natl. Acad. Sci. USA* **1944**, *30*, 2344.
(28) d'Amour, H.; Schiferl, D.; Denner, W.; Schulz, H.; Holzapfel, W. B. *J. Appl. Phys.* **1978**, *49*, 4411.
(29) Methfessel, M.; Paxton, A. T. *Phys. Rev. B* **1989**, *40*, 3616.
(30) Blöchl, P. E.; Jepsen, O.; Andersen, O. K. *Phys. Rev. B* **1994**, *49*, 16223.
(31) Nosé, S. *J. Chem. Phys.* **1984**, *81*, 511.
(32) Chen, P. J.; Colaianni, M. L.; Yates, J. T., Jr. *Phys. Rev. B* **1990**, *41*, 8025.
(33) Wander, A.; Searle, B.; Harrison, N. M. *Surf. Sci.* **2000**, *458*, 25.
(34) Baxter, R.; Reinhardt, P.; López, N.; Illas, F. *Surf. Sci.* **2000**, *445*, 448.
(35) Mackrodt, W. C.; Davey, R. J.; Black, S. N. *J. Cryst. Growth* **1987**, *80*, 441.
(36) Manassidis, I.; De Vita, A.; Gillan, M. J. *Surf. Sci. Lett.* **1993**, *285*, L517. Manassidis, I.; Gillan, M. J. *J. Am. Ceram. Soc.* **1994**, *77*, 335.
(37) Causà, M.; Dovesi, R.; Pisani, C.; Roetti, C. *Surf. Sci.* **1989**, *215*, 259.

(38) Tasker, P. W. Structure and Properties of MgO and Al_2O_3 Ceramics. In *Advances in Ceramics*; Kingery, W. D., Ed.; The American Ceramic Society, Inc.: Columbus, 1984; Vol. 10, p. 176.
(39) Blonski, S.; Garofalini, S. H. *Surf. Sci*. **1993**, *295*, 263.
(40) Kruse, C.; Finnis, M. W.; Milman, V. Y.; Payne, M. C.; De Vita, A.; Gillan, M. J. *J. Am. Ceram. Soc*. **1994**, *77*, 431.
(41) Puchin, V. E.; Gale, J. D.; Shluger, A. L.; Kotomin, E. A.; Günster, J.; Brause, M.; Kempter, V. *Surf. Sci*. **1997**, *370*, 190.
(42) Verdozzi, C.; Jennision, D. R.; Shultz, P. A.; Sears, M. P. *Phys. Rev. Lett.* **1999**, *82*, 799.
(43) Rhee, S. K. *J. Am. Ceram. Soc*. **1972**, *55*, 300.
(44) Becke, A. D.; Edgecombe, K. E. *J. Chem. Phys*. **1990**, *92*, 5397.
(45) Savin, A.; Jepsen, O.; Flad, J.; Anderson, O. K.; Preuss, H.; von Schneiring, H. G. *Angew. Chem., Int. Engl*. **1992**, *31*, 187.
(46) De Santis, L.; Resta, R. *Surf. Sci*. **2000**, *450*, 126.
(47) Bart, F.; Guittet, M. J.; Henriot, M.; Thromat, N.; Gautier, M.; Duraud, J. P. *J. Electron Spectrosc. Relat. Phenom.* **1994**, *69*, 245.
(48) Ciraci, S.; Batra, I. P. *Phys. Rev. B* **1983**, *28*, 982.